AJNR

Preoperative assessment of meningioma consistency using a combination of magnetic resonance elastography and diffusion tensor imaging

Yuting Bao, Suhao Qiu, Zhenyu Li, Guangzhong Yang, Yuan Feng and Qi Yue

AJNR Am J Neuroradiol published online 21 June 2024
http://www.ajnr.org/content/early/2024/06/21/ajnr.A8385

ORIGINAL RESEARCH

Preoperative assessment of meningioma consistency using a combination of magnetic resonance elastography and diffusion tensor imaging

Yuting Bao[1,2,3,4,5], Suhao Qiu[6,7,8], Zhenyu Li[1,2,3,4,5], Guangzhong Yang[6,7,8], Yuan Feng[6,7,8,9], Qi Yue[1,2,3,4,5]

ABSTRACT

BACKGROUND AND PURPOSE: Preoperative assessment of meningioma consistency is beneficial for optimizing surgical strategy and prognosis of patients. We aim to develop a non-invasive prediction model for meningioma consistency utilizing magnetic resonance elastography (MRE) and diffusion tensor imaging (DTI).

MATERIALS AND METHODS: Ninety-four patients (52yr ± 22, 69 females, 25 males) diagnosed with meningioma were recruited in the study. Each patient underwent preoperative T1-weighted imaging (T1WI), T2-weighted imaging (T2WI), DTI, and MRE. Combined MRE-DTI model was developed based on multiple logistic regression. Intraoperative tumor descriptions served as clinical criteria for evaluating meningioma consistency. The diagnostic efficacy in determining meningioma consistency was evaluated using receiver operating characteristic (ROC) curve. Further validation was conducted in twenty-seven stereotactic biopsies using indentation tests and underlying mechanism was investigated by histologic analysis.

RESULTS: Among all the imaging modalities, MRE demonstrated the highest efficacy with the shear modulus magnitude (|G*|) achieving an area under the curve (AUC) of 0.81 (95% CI: 0.70-0.93). When combined with DTI, the diagnostic accuracy further increased (AUC: 0.88, 95% CI: 0.78-0.97), surpassing any modality alone. Indentation measurement based on stereotactic biopsies further demonstrated that the MRE-DTI model was suitable for predicting intra-tumor consistency. Histological analysis suggested that meningioma consistency may be correlated with tumor cell density and fibrous content.

CONCLUSIONS: The MRE-DTI combined model is effective in noninvasive prediction of meningioma consistency.

ABBREVIATIONS: MRE = magnetic resonance elastography; FA = fractional anisotropy; ROC = receiver operating characteristic; AUC = area under curve.

Received April 11, 2024; accepted after revision June 06, 2024.
From the Department of Neurosurgery (Y.B., Z.L., Q.Y.), Huashan Hospital, Shanghai Medical College, Fudan University, Shanghai, China; National Center for Neurological Disorders (Y.B., Z.L., Q.Y.), Shanghai, China; Shanghai Key Laboratory of Brain Function and Restoration and Neural Regeneration (Y.B., Z.L., Q.Y.), Fudan University, Shanghai, China; Neurosurgical Institute of Fudan University (Y.B., Z.L., Q.Y.), Shanghai, China; Shanghai Clinical Medical Center of Neurosurgery (Y.B., Z.L., Q.Y.), Shanghai 200040, China; School of Biomedical Engineering (S.Q., G.Y., Y.F.), Shanghai Jiao Tong University, Shanghai, China; Institute of Medical Robotics (S.Q., G.Y., Y.F.), Shanghai Jiao Tong University, Shanghai, China; National Engineering Research Center of Advanced Magnetic Resonance Technologies for Diagnosis and Therapy (NERC-AMRT) (S.Q., G.Y., Y.F.), Shanghai Jiao Tong University, Shanghai, China, and Department of Radiology(Y.F.), Ruijin Hospital affiliated to Shanghai Jiao Tong University School of Medicine, Shanghai, China.

Yuting Bao, Suhao Qiu and Zhenyu Li contributed equally to this study.

The authors declare no conflicts of interest related to the content of this article.

Please address correspondence to Qi Yue, MD, Department of Neurosurgery, Huashan Hospital, Fudan University, No.12 Middle Wulumuqi Rd, Shanghai, China; e-mail: yueqi1989@126.com.

SUMMARY SECTION

PREVIOUS LITERATURE: MR imaging techniques have been employed for predicting the consistency of intracranial meningiomas. T2WI and DTI derived FA have been validated as predictors of meningioma consistency. Meanwhile, studies of MRE on brain tumors show the potential of using biomechanical properties to evaluate the tumor consistency.

KEY FINDINGS: MRE demonstrated the highest efficacy in diagnosing meningioma consistency compared with T1WI, T2WI and DTI. When combined, MRE-DTI model showed better accuracy in predicting tumor consistency, which was further confirmed by indentation measurement based on stereotactic biopsies.

KNOWLEDGE ADVANCEMENT: The MRE-DTI model achieved highest diagnostic efficiency of meningioma consistency compared with each modality alone. Stereotactic biopsies and voxel-wise analysis have verified the application of the MRE-DTI combined model in determining intratumoral heterogeneity. Quantitative measurements of tumor consistency were obtained through indentation tests, which serve as reliable criteria.

Copyright 2024 by American Society of Neuroradiology.

INTRODUCTION

Meningioma is the most common type of primary intracranial tumor, originating in the arachnoid and typically exhibiting slow growth, often remaining undiagnosed for years.[1,2] Surgical resection is the primary treatment for most cases of meningioma.[3,4] Various intraoperative and postoperative risks are known to be associated with tumor characteristics such as consistency, adhesions, and homogeneity,[5-8] particularly in cases where the tumor's location presents challenges for access and resection.[9] Therefore, accurate preoperative evaluation of intraoperative tumor conditions is valuable for guiding surgical strategy and risk assessment.

Magnetic resonance imaging (MRI) has been widely utilized in the diagnosis of meningiomas.[10,11] Research efforts have focused on leveraging both conventional and advanced MRI sequences as predictors of meningioma consistency. [4,9,10,12-15] Diffusion tensor imaging (DTI) derived fractional anisotropy (FA) and mean diffusivity (MD) maps have been validated as predictors of meningioma consistency. Notably, FA has been shown to outperform T2-weighted imaging (T2WI) as a predictor.[16] However, certain studies have not replicated these findings.[17] Additionally, both T2WI and DTI alone can reliably predict consistency only in a small number of extremely soft or firm meningiomas, significantly limiting their clinical applicability.[18]

Magnetic resonance elastography (MRE) is a phase contrast-based MRI technique that visualizes the propagation of mechanical waves in tissues, enabling noninvasive determination of tissue consistency.[5,19-21] While preliminary MRE research have been conducted in human organs such as breast,[22,23] prostate,[24] liver,[25] and skeletal muscle,[26] studies in brain MRE gained momentum following reports correlating tumor elasticity assessed by MRE with tumor consistency based on surgical findings.[27,28] It has been demonstrated that the biomechanical properties of intracranial tumors measured by MRE significantly correlating with tumor consistency.[5,17,18,29-31] Nevertheless, limited studies have compared the in vivo measurement with intraoperative assessment and validated with ex vivo biomechanical testing. In addition, enhancing the predictive ability of MRE with other modalities remains an area of active investigation.[32]

In this study, we devised a multimodal approach that integrates |G*| in MRE and FA values in DTI to predict the consistency of intracranial meningiomas. Stereotactic biopsies as well as voxel-wise analysis were performed to verify the application of the MRE-DTI combined model in determining intratumoral heterogeneity. Quantitative measurements of tumor consistency were obtained through indentation tests to validate the performance.

MATERIALS AND METHODS

Population

Study participants were prospectively recruited from patients diagnosed with meningioma preoperatively by experienced radiologists and confirmed by biopsies from June 2022 to October 2023. The study protocol was approved by the Institutional Review Board, and informed consent in written form was obtained from all participants. Pathologic diagnoses were determined according to the 2021 World Health Organization (WHO) classification of central nervous system (CNS) tumors.[33] Exclusion criteria were listed in the Online Supplemental Data.

Imaging acquisition

MRI scanning was performed within a week prior to surgery. All MRI sequences including T1WI, T2WI, DTI, MRE were acquired using a 3.0 T MRI system (uMR790, United Imaging Healthcare, Shanghai, China). The imaging protocol are shown in Online Supplemental Data.

Image and data processing

Once all MRI acquisition and construction have been completed, the MRE, DTI and T2WI results were aligned to the T1WI, which was the uniform standard space. Detailed information regarding MRI construction is provided in Online Supplemental Data.

For the delineation of brain tumors, two physicians independently delineated ROIs for the lesions layer by layer according to the uniform standard space images and created 3D segmentations of the tumor. The ROIs referring to tumor area were then applied on the map of each MR sequence. Any consequential discrepancies were resolved through discussion to achieve a consensus. The ROIs referring to tumor area were then applied on the map of each MR sequence. Signal intensity (SI) in T1WI, T2WI[10,17] and FA value in DTI and |G*| value in MRE was analyzed by software ITK-SNAP (4.0, Penn Image Computing and Science Laboratory, Philadelphia, USA).[34] Tumor consistency was then calculated as the pixel contained in each ROI and averaged across all ROIs. The SI ratio (tumor to cerebral cortex SI) on T1WI and T2WI was employed for further evaluation.[35] For the SI of the cortex, a ROI (6 - 9 mm3) was placed within the contralateral superior frontal gyrus.[36]

Surgery and intraoperative evaluation

Two surgeon specialists in brain surgery (22 and 16 years of experience, respectively) primarily conducted all surgical resections, and their intraoperative impressions of tumor consistency served as reference standards for later analysis. Both experts were blinded to MRI data. All detailed descriptions were recorded in surgical documents. Tumor consistency was graded on the following scale: 1) soft: removed totally with suction; 2) mostly soft: removed mostly with suction; 3) medium: removed with combination of suction and ultrasonic aspirator intensity <40; 4) tenacious: removed with ultrasonic aspirator intensity between 40 and 70; 5) hard: removed with ultrasonic aspirator intensity >70 or other sharp dissection surgical adjuncts.[4,14,29] The multiple categorizations of tumor consistency were reduced to two categories for further model accuracy assessment, as consistent with previous studies in which tumor consistency was first graded in multiple categories and then dichotomized for model accuracy assessment.[16,17,37] It is hypothesized that the efficiency of models in

diagnosing tumor consistency based on dichotomies is a prerequisite for their further prediction of multiple consistency grading. In this case, “soft”, “mostly soft” and “medium” meningiomas that can be removed by suction were categorized as “Soft” (corresponding to grades 1 and 2 of Zada’s consistency grading system), whereas “tenacious” and “hard” meningiomas that can only be removed by ultrasonic aspiration were categorized as “Firm” (corresponding to grades 3, 4 and 5 of Zada's consistency grading system).

For the biopsies to verifying of modality, specimens of the tumor were resected separately during the operation with their exact locations recorded according to the intra-navigation. The consistency of each specimen was then graded individually. The acquired images from scanned MRI sequences were aligned with the intra-navigation images, where each biopsy location was marked. Subsequently, the ROI was delineated for voxel-wise analysis.

Indentation measurement

A custom-built indentation device in a previous study was used to measure the tissue consistency of tumor samples ex vivo.[38] Surgical specimens were taken from different regions of each tumor and the indentation measurement was conducted within thirty minutes after the sample was acquired. A ramp-hold indentation protocol was accepted in this test.[39] Details of the procedure and algorithm can be found in Online Supplemental Data. Eventually, instantaneous shear modulus (G_0) was employed as the result of the indentation measurement.

Pathologic assessments

After the surgical specimens underwent indentation tests, tissue samples were collected for pathological analysis. After formalin fixation and paraffin embedding, the tissues were stained with hematoxylin and eosin (H&E) stain and Masson stain. Tissue slides from various tumor areas were scanned digitally using a VS200 whole-slide image scanner (Olympus, Japan) and OlyVIA software 4.1.1 at 20x magnification. Quantitative histologic parameter of tumor cellularity and fibrous content was obtained by computer-assisted analysis using ImageJ (v6.0.0.260; Media Cybernetics Inc, Rockville, MD, USA).[17] The average number of cell nuclei in per unit area was calculated as the cell density. Cell counting and fibrous content calculation was performed on each sample three times.

Statistical methods

Statistical analyses and graphical visualization were performed by using GraphPad Prism 9.0 (GraphPad Software Inc, San Diego, CA, USA). The MRI variable distribution was initially assessed using the Shapiro-Wilk test. For normally distributed data, a two-tailed independent samples t-test was conducted, while for non-normally distributed data, a Mann-Whitney test was performed. The receiver operating characteristic (ROC) curve analysis was plotted by connecting points with a coordinate of the false positive rate (1 − specificity) and the true positive rate (sensitivity) for the classifiers using various thresholds. ROC curves were compared using the DeLong test. Areas under ROC curves (AUCs) were then analyzed to compare levels of diagnostic performance by each modality in detecting tumor consistency. Confusion matrices are also used as a statistical tool to assess the effectiveness of each predictive models. The linear relationships between TIWI, T2WI, FA and |G*| were further assessed using the Pearson correlation coefficient. Multiple logistic regression with two-way interactions (consistency ~ Intercept + FA + |G*| + FA: |G*|， β0: -21.67; β1: 43.57; β2: 0.01007; β3: -0.01946) was utilized to construct combined models based on features derived from TIWI, T2WI, DTI and MRE data. Statistical significance level was set at $P < 0.05$.

RESULTS

Demographics

Fig 1 demonstrated the flow chart of the study. The patient characteristics are summarized in Online Supplemental Data. Overall, 94 patients consisted of 25 male and 69 female were enrolled in this study, of whom the average age was 54 ±22 years. Most of the patients reported dizziness and headache as their primary symptom (38.3%), followed by physical health examination (30.9%), epilepsy (10.6%), and local neurological deficits (11.7%). Pathological diagnoses included 84 typical (grade 1) meningiomas and 10 atypical (grade 2) meningiomas. The typical meningiomas included the fibroblastic (34.0%), transitional (10.6%), meningothelial (38.3%), angiomatous (5.3%), and secretory (1.1%) tissue types. Moreover, total resection was achieved in most of the tumors.

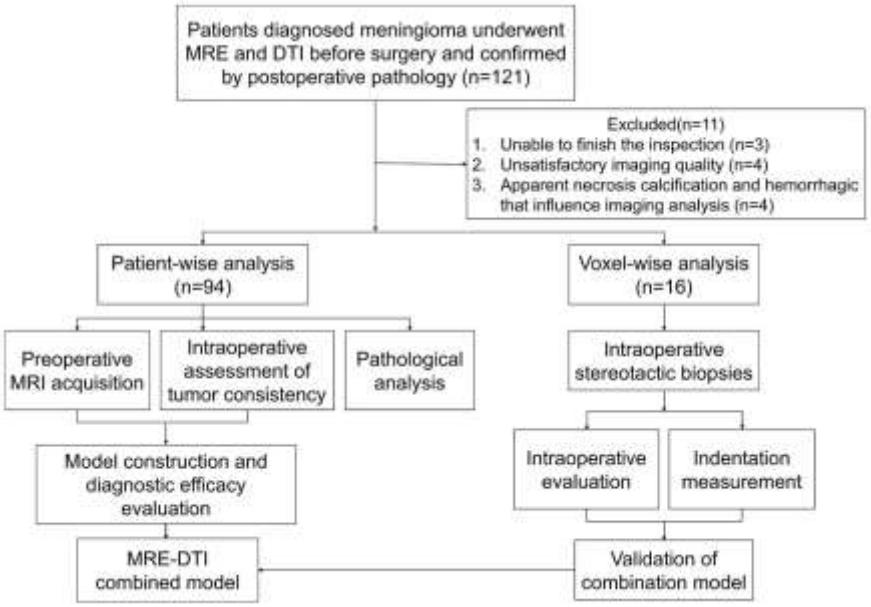

FIG 1. Flow chart for the inclusion and exclusion criteria in the study cohort. MRE, Magnetic Resonance Elastography; DTI, Diffusion Tensor Imaging.

Radiological and intraoperative findings

Representative images of T1WI, T2WI, FA map in DTI and |G*| map in MRE is exhibited in Fig 2, including one patient with a soft meningioma and one with a firm meningioma. For all the images acquired, the average signal intensity (SI) of delineated ROIs on FA map and |G*| map as well as SI ratio (tumor to cerebral cortex SI) on T1WI and T2WI were calculated and compared in "Soft" and "Firm" groups, as listed in Online Supplemental Data. The results showed that the |G*| between two groups was statistically significant (P < 0.001), while there were no significant differences of T1WI, T2WI and FA between two groups. Additionally, the correlation analysis demonstrated that |G*| was an independent variable from T1WI, T2WI and FA (Online Supplemental Data).

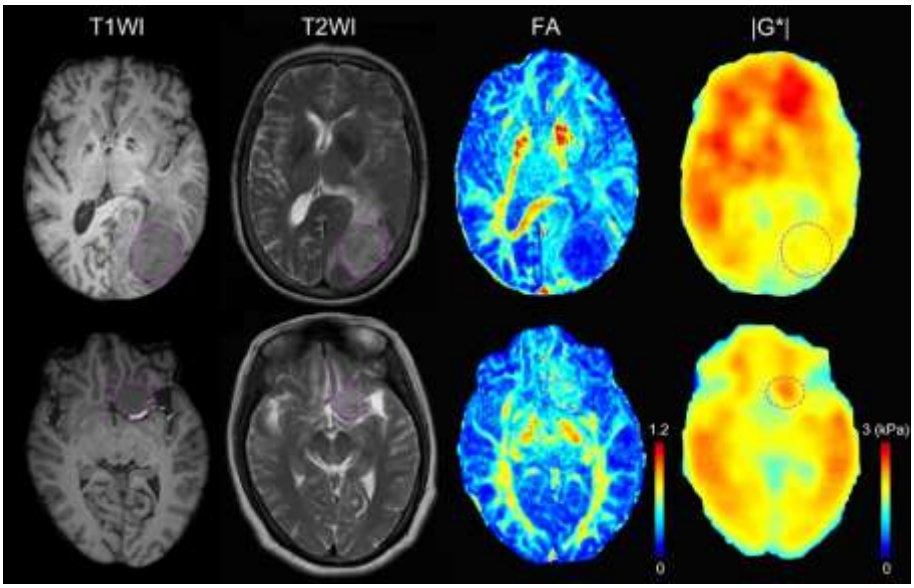

FIG 2. A 66-year-old female patient with soft meningioma (upper) in the left occipital lobe and a 58-year-old female patient with hard meningioma (lower) in the left sphenoid ridge. The tumor ROIs were delineated with purple dashed lines in T1WI, T2WI, FA and |G*| images from left to right.

Predictive accuracy of single modality and combined model

The ROC curve was conducted based on mean SI calculated from ROI of tumor in each modality. The results of each individual modality and the combined modality are presented in Fig 3. The |G*| demonstrated the best diagnostic efficiency in singular modalities, with AUC of 0.81(95% CI: 0.70-0.93), followed by FA (AUC: 0.66, 95% CI: 0.53-0.79), T2WI (AUC: 0.63, 95%CI: 0.51 to 0.77), while T1WI failed to predict tumor consistency (AUC: 0.51, 95%CI: 0.37 to 0.65). Furthermore, the use of combined modalities demonstrated significantly greater performance in determining meningioma consistency compared to single modalities. Notably, combined |G*|-FA exhibited the highest level of predictive accuracy with an AUC of 0.88 (95%CI: 0.78 to 0.97), closely tied with |G*|-T1WI (AUC: 0.82, 95% CI: 0.71

to 0.93) and |G*|-T2WI (AUC: 0.82, 95% CI: 0.71 to 0.93). To consistent with, the confusion metrics of each model yielded a similar outcome (Online Supplemental Data).

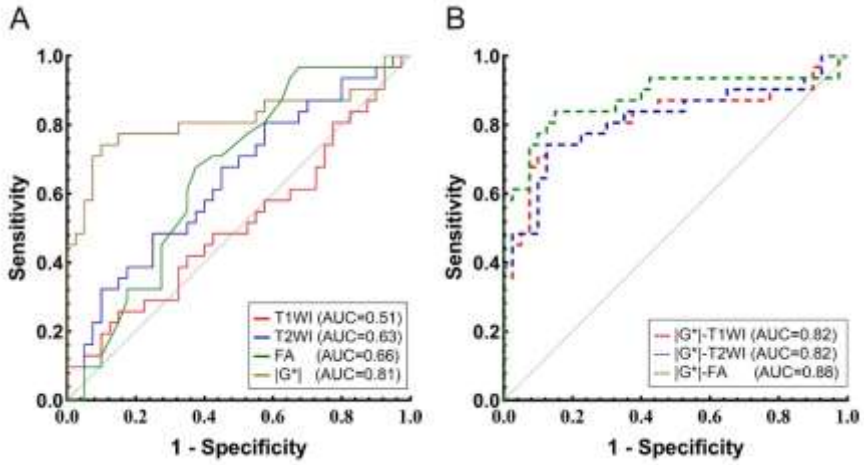

FIG 3. Comparison of diagnostic performance of modalities in evaluating meningioma consistency: (A) ROC curves based on T1WI, T2WI, FA, and |G*|; (B) ROC curves based on combinations of |G*|-T1WI, |G*|-T2WI, |G*|-FA.

Voxel-wise validation in stereotactic biopsies using indentation measurement

Considering the heterogeneity of tumors, we performed 27 intratumoral stereotactic biopsies in 16 patients to further assess the reliability of the |G*|-FA combination by voxel-wise analysis. The SI of ROI in each specimen's precise location, as recorded according to intra-navigation, was calculated, and matched with the intraoperative records (Online Supplemental Data). Representative images of biopsy localization and H&E staining of specimen was displayed in Online Supplemental Data. The voxel-wise analysis showed that |G*|-FA combination was strongly correlated with intraoperative assessment of tumor consistency (P = 0.004, Fig 4A). Moreover, the indentation test was introduced as an objective criterion for assessing tumor consistency. The correlation analysis confirmed that the indentation measurement exhibited a substantial link with intraoperative evaluation (P < 0.001, Fig 4B). Therefore, the indentation measurement was employed to further validate the efficiency of the |G*|-FA combination. The combined modality showed a significant correlation with indentation results ((P = 0.004, Fig 4C). Furthermore, a good correlation has been found in correlation analysis between indentation measurement and |G*| (P < 0.001, Online Supplemental Data).

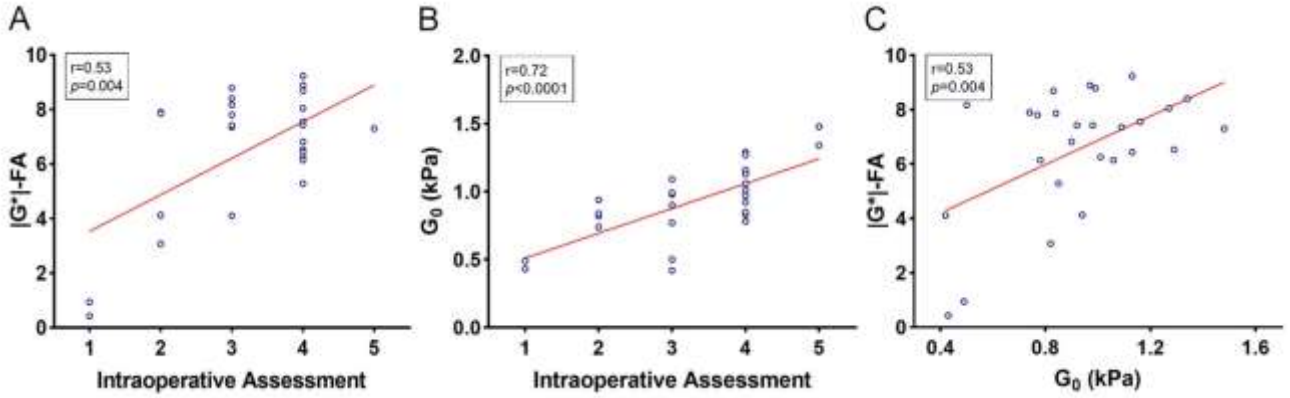

FIG 3. Correlation analysis between (A) |G*|-FA and intraoperative assessment (r = 0.53, P = 0.004); (B) indentation measurement (G_0) and intraoperative assessment (r = 0.72, P < 0.001); (C) |G*|-FA and indentation measurement (G_0) (r = 0.53, P = 0.004).

Histologic analysis to investigate underlying mechanism

After performing an indentation test, histologic analysis was conducted on each specimen. Variability in tumor cellularity and fibrous content was observed among individual samples. Quantitative analysis of specimens indicated that the firm group possessed significantly higher cell density (P = 0.02, Online Supplemental Data) and larger fibrous content (P = 0.04, Online Supplemental Data). It indicated potential correlation between tumor consistency and its pathological features, which could be identified by the presentation of the tumor on MRI. This section may be divided into subsections if it facilitates reading the paper. Do not mix results and discussion into this section. Present results in a clear, orderly fashion, and include statistical findings to substantiate the results.

DISCUSSION

In this study, we explored the diagnostic efficiency of combined MR modalities compared with single ones in predicting meningioma consistency. Indentation testing based on stereotactic biopsies further confirmed the generalizability of the patient-wise developed model

in intratumoral voxel-wise prediction. The results demonstrated the MRE-DTI model may be potentially practical for preoperatively assessing the tumor characteristics, which can help to optimize surgical strategies and predict operative risks, thereby minimizing the incidence of surgical complications and recurrence, and significantly improving the quality of surgery and patients' prognosis.

MR imaging techniques have been employed for predicting the consistency of intracranial meningiomas. Early studies found tumors showing hyperintense in T2W images were more likely correlate with soft consistency ($P < 0.01$) but no correlation was between T1WI and tumor consistency.[10] Furthermore, the FA value from DTI was found to be a significant independent predictor of tumor consistency ($P < 0.01$).[14] Consistent with these results, Romani et al. (2014) concluded that isointense signal on MD maps ($P < 0.01$) and FA value > 0.3 ($P < 0.001$) were significant indicators for predicting hard-consistency tumors.[16] Nevertheless, there is no consensus on using MRI to determine tumor consistency.[12,14,16-18,35,37] Meanwhile, early MRE studies on brain tumors show the potential of using biomechanical properties to evaluate the consistency.[27] In our study, it was confirmed that MRE exhibited better predictive accuracy than other MR modalities. Additionally, while MD showed a moderate diagnostic efficiency in diagnosing tumor consistency with AUC of 0.63, its combination with |G*| (AUC: 0.82, 95%CI: 0.71 to 0.93, Online Supplemental Data) did not demonstrated elevated efficacy compared with |G*|.

Recently, multimodal MR imaging has emerged as a potential tool for prediction of tumor consistency. A combined T1WI and T2WI for assessment showed a sensitivity of 90% and 56% ($P < 0.001$) for detecting soft and firm meningiomas, respectively.[4] Furthermore, a three-dimensional (3D) combination and display of multimodality images have been suggested to enhance the accuracy of interpreting cranial base tumors, potentially improving the safety of clinical procedures.[40] Additionally, MRI radiomics is regarded as a potential tool for the surgical risk evaluation of meningiomas.[41] Zhai et al. demonstrated that radiomic analysis based on T1CE of meningioma cases is a reliable predictor of tumor consistency.[42] This suggests that radiomic analysis can be a valuable tool for the preoperative assessment of meningiomas. Despite these promising outcomes, the validation of the accuracy of such models in real practice has yet to be demonstrated. In this study, the combination of FA and |G*| can effectively predict the consistency of meningiomas with favorable accuracy preoperatively, with an AUC of 0.88, surpassing the performance of each modality alone. Meanwhile, the correlation coefficients presented by the voxel-wise analysis, although not particularly high, demonstrated a significant correlation between the |G*|-FA combination and tumor consistency.

Given that heterogeneity of meningioma is an essential factor contributing to differences in surgical strategy and prognosis, it is crucial to precisely describe the consistency of tumor based on its exact intratumoral location.[5,29] Hence, we conducted voxel-wise analysis based on stereotactic biopsies to further validate the practical reliability of combined model, where consistency of each tumor specimen was quantitatively measured by indentation test and calculated according to each modality. Our study revealed a strong correlation between the results of the combined model and tumor consistency, suggesting that the MRE-DTI model based on patient-wise analysis could be implemented for voxel-wise intratumoral diagnosis.

As neuroimaging techniques continue to advance, offering more effective modalities for evaluating tumor consistency, the development of a precise and unbiased tumor consistency scoring system would greatly enhance our capacity to analyze and communicate surgical parameters regarding tumor consistency in a standardized manner. Previous studies have employed grading scales of meningioma consistency according to the surgical instruments used and the working mode of the surgical instruments, or the differences in the ways of tumor resection. Zada et al proposed a 5-point scale grading system that relies on the ability of internal debulking and stiffness of the tumor capsule of the meningioma.[43] It showed high agreement with a kappa score of 0.87. Hughes et al graded meningioma consistency mainly based on which tool was utilized during tumor resection.[29] The scale is straightforward but lacks quantitative criteria. Takamura et al defined intraoperative tumor consistency based on the Clarity Ultrasonic Surgical Aspirator (CUSA) amplitude applied for tumor removal.[44] The grading criteria employed in this study were based on the instrument used in the operation and its working mode, which were widely used by surgeons. It is admittedly that diverse scales applied in researches provides the possibility of discrepancies and inter-user disagreements in determining tumor consistency for there is currently no uniform grading system for the consistency of meningiomas. Given that, we proposed the indentation measurement as quantitative technique for meningioma consistency evaluation. The correlation analysis between intraoperative evaluation and indentation measurements in our study demonstrated that objective assessments from experienced experts are consistent and reliable.

Studies have employed novel techniques to assess the consistency of brain tumors. Della Pepa et al introduced intraoperative ultrasound (IOUS) elastography as a real-time imaging technique in the intraoperative prediction of meningioma consistency and brain-meningioma interface assessment.[45] Due to the difficulty of obtaining images that match the standard radiological planes and maintaining correct intraoperative spatial localization associated with it, the practicality of this technique remains to be demonstrated. Abramczyk et al utilized an indentation test for evaluating mechanical properties of high-grade medulloblastoma and identified significant variation in the mechanical properties of the tumor tissue.[46] Additionally, a positive correlation was found between tissue consistency and pathological grading of gliomas.[47] In this study, we evaluated the accuracy of using indentation measurement as a quantitative determinant for meningioma consistency. The results indicated a substantial correlation between indentation results and intraoperative grading assessments, suggesting that indentation measurement can serve as an objective and reliable reference for estimating tumor consistency. According to the correlation analysis, the |G*|-FA combination exhibited a significant association with indentation outcomes.

Studies have reported a correlation between the consistency of meningiomas and their histopathology, with fibrous meningiomas more likely to be classified as stiff tumors.[44] Recent studies demonstrated the impact of hypercellularity on shear stiffness in MRE, noting elevated shear stiffness in densely cellular meningothelial tumors.[17] In our current study, we examined the variation of cellular density and fibrous content in soft and firm tumors. The results revealed that both factors were associated with tumor consistency, which may be reflected in imaging. Additionally, fibroblastic meningiomas exhibited higher FA values in DTI compared to other subtypes (Online Supplemental Data). It should be noted that the term "Fibrous content", which refers to the fibrous content of each tumor specimen as assessed by Masson staining, does not correspond to the pathological subtype of meningioma known as "fibroblastic". Fibroblastic meningiomas are characterized by spindle-shaped tumor cells, with narrow rod-shaped nuclei. These cells are embedded in abundant

collagenous or reticulum background. Therefore, it does not mean that the fibrous content of fibroblastic meningioma is necessarily higher than that of other meningioma subtypes. The consistency of meningiomas may be related to the fibrous content, but not to the pathological subtype. Nevertheless, future studies will investigate the underlying mechanobiological mechanisms of meningioma consistency.

There are several limitations in this study. Firstly, as a proof-of-concept study, only GRAPPA was used for the MRE scan with no further acceleration techniques. Therefore, the total scan time was ~18min. In fact, improved imaging protocol with accelerated sequence and reconstruction algorithm can significantly reduce the scan time. For example, if imaging the tumor area only with a single frequency, less than four minutes is needed. Secondly, only a limited number of tissue samples were obtained and validated using the indentation measurement and histologic analysis. Thirdly, T1 mapping or T2 mapping was not performed to obtain absolute values for quantification. Future work includes measurements with an enlarged sample size with ex vivo testing, and integration of novel modalities such as MR fingerprinting.

CONCLUSIONS

The MRE-DTI model proves to be a better predictor of meningioma consistency compared to other MR modalities (T1WI, T2WI, DTI) used alone or combined. In clinical practice, it could serve as an effective tool for preoperative assessment of tumor consistency, thus guiding the decision making of surgical strategy and assessment of surgical risk. With its help, maximum safety of resection as well as preservation of neurological function may be achieved to reduce tumor recurrence and improve patients' prognosis.

ACKNOWLEDGMENTS

The authors wish to thank the patients for participating in this study.

REFERENCES

1. Riemenschneider MJ, Perry A, Reifenberger G. Histological classification and molecular genetics of meningiomas. *Lancet Neurol.* Dec 2006;5(12):1045-1054. DOI: http://dx.doi.org/10.1016/s1474-4422(06)70625-1
2. Ostrom QT, Cioffi G, Gittleman H, et al. CBTRUS Statistical Report: Primary Brain and Other Central Nervous System Tumors Diagnosed in the United States in 2012-2016. *Neuro-oncology.* 2019;21(Suppl 5). DOI: http://dx.doi.org/10.1093/neuonc/noz150
3. Yao A, Pain M, Balchandani P, Shrivastava RK. Can MRI predict meningioma consistency?: a correlation with tumor pathology and systematic review. *Neurosurg Rev.* Jul 2018;41(3):745-753. DOI: http://dx.doi.org/10.1007/s10143-016-0801-0
4. Hoover JM, Morris JM, Meyer FB. Use of preoperative magnetic resonance imaging T1 and T2 sequences to determine intraoperative meningioma consistency. *Surg Neurol Int.* 2011;2:142. DOI: http://dx.doi.org/10.4103/2152-7806.85983
5. Aunan-Diop JS, Halle B, Pedersen CB, et al. Magnetic Resonance Elastography in Intracranial Neoplasms: A Scoping Review. *Top Magn Reson Imaging.* Feb 1 2022;31(1):9-22. DOI: http://dx.doi.org/10.1097/RMR.0000000000000292
6. Little KM, Friedman AH, Sampson JH, Wanibuchi M, Fukushima T. Surgical management of petroclival meningiomas: defining resection goals based on risk of neurological morbidity and tumor recurrence rates in 137 patients. *Neurosurgery.* Mar 2005;56(3):546-559; discussion 546-559. DOI: http://dx.doi.org/10.1227/01.neu.0000153906.12640.62
7. Sekhar LN, Jannetta PJ, Burkhart LE, Janosky JE. Meningiomas involving the clivus: a six-year experience with 41 patients. *Neurosurgery.* Nov 1990;27(5):764-781; discussion 781.
8. Yin Z, Lu X, Cohen Cohen S, et al. A new method for quantification and 3D visualization of brain tumor adhesion using slip interface imaging in patients with meningiomas. *Eur Radiol.* Aug 2021;31(8):5554-5564. DOI: http://dx.doi.org/10.1007/s00330-021-07918-6
9. Sitthinamsuwan B, Khampalikit I, Nunta-aree S, Srirabheebhat P, Witthiwej T, Nitising A. Predictors of meningioma consistency: A study in 243 consecutive cases. *Acta Neurochir (Wien).* Aug 2012;154(8):1383-1389. DOI: http://dx.doi.org/10.1007/s00701-012-1427-9
10. Chen TC, Zee CS, Miller CA, et al. Magnetic resonance imaging and pathological correlates of meningiomas. *Neurosurgery.* Dec 1992;31(6):1015-1021; discussion 1021-1012. DOI: http://dx.doi.org/10.1227/00006123-199212000-00005
11. Zimmerman RD, Fleming CA, Saint-Louis LA, Lee BC, Manning JJ, Deck MD. Magnetic resonance imaging of meningiomas. *AJNR Am J Neuroradiol.* Mar-Apr 1985;6(2):149-157.
12. Carpeggiani P, Crisi G, Trevisan C. MRI of intracranial meningiomas: correlations with histology and physical consistency. *Neuroradiology.* 1993;35(7):532-536. DOI: http://dx.doi.org/10.1007/BF00588715
13. Yamaguchi N, Kawase T, Sagoh M, Ohira T, Shiga H, Toya S. Prediction of consistency of meningiomas with preoperative magnetic resonance imaging. *Surg Neurol.* Dec 1997;48(6):579-583. DOI: http://dx.doi.org/10.1016/s0090-3019(96)00439-9
14. Kashimura H, Inoue T, Ogasawara K, et al. Prediction of meningioma consistency using fractional anisotropy value measured by magnetic resonance imaging. *J Neurosurg.* Oct 2007;107(4):784-787. DOI: http://dx.doi.org/10.3171/JNS-07/10/0784
15. Shiroishi MS, Cen SY, Tamrazi B, et al. Predicting Meningioma Consistency on Preoperative Neuroimaging Studies. *Neurosurg Clin N Am.* Apr 2016;27(2):145-154. DOI: http://dx.doi.org/10.1016/j.nec.2015.11.007
16. Romani R, Tang WJ, Mao Y, et al. Diffusion tensor magnetic resonance imaging for predicting the consistency of intracranial meningiomas. *Acta Neurochir (Wien).* Oct 2014;156(10):1837-1845. DOI: http://dx.doi.org/10.1007/s00701-014-2149-y
17. Shi Y, Huo Y, Pan C, et al. Use of magnetic resonance elastography to gauge meningioma intratumoral consistency and histotype. *Neuroimage Clin.* 2022;36:103173. DOI: http://dx.doi.org/10.1016/j.nicl.2022.103173
18. Murphy MC, Huston J, 3rd, Glaser KJ, et al. Preoperative assessment of meningioma stiffness using magnetic resonance elastography. *J Neurosurg.* Mar 2013;118(3):643-648. DOI: http://dx.doi.org/10.3171/2012.9.JNS12519
19. Muthupillai R, Lomas DJ, Rossman PJ, Greenleaf JF, Manduca A, Ehman RL. Magnetic resonance elastography by direct visualization of propagating acoustic strain waves. *Science.* Sep 29 1995;269(5232):1854-1857. DOI: http://dx.doi.org/10.1126/science.7569924
20. Sack I. Magnetic resonance elastography from fundamental soft-tissue mechanics to diagnostic imaging. *Nature Reviews Physics.* 2023/01/01

2023;5(1):25-42. DOI: http://dx.doi.org/10.1038/s42254-022-00543-2

21. Bunevicius A, Schregel K, Sinkus R, Golby A, Patz S. REVIEW: MR elastography of brain tumors. *NeuroImage. Clinical*. 2020;25:102109. DOI: http://dx.doi.org/10.1016/j.nicl.2019.102109
22. Sinkus R, Tanter M, Catheline S, et al. Imaging anisotropic and viscous properties of breast tissue by magnetic resonance-elastography. *Magn Reson Med.* Feb 2005;53(2):372-387. DOI: http://dx.doi.org/10.1002/mrm.20355
23. McKnight AL, Kugel JL, Rossman PJ, Manduca A, Hartmann LC, Ehman RL. MR elastography of breast cancer: preliminary results. *AJR Am J Roentgenol.* Jun 2002;178(6):1411-1417. DOI: http://dx.doi.org/10.2214/ajr.178.6.1781411
24. Kemper J, Sinkus R, Lorenzen J, Nolte-Ernsting C, Stork A, Adam G. MR elastography of the prostate: initial in-vivo application. *Rofo.* Aug 2004;176(8):1094-1099. DOI: http://dx.doi.org/10.1055/s-2004-813279
25. Rouviere O, Yin M, Dresner MA, et al. MR elastography of the liver: preliminary results. *Radiology.* Aug 2006;240(2):440-448. DOI: http://dx.doi.org/10.1148/radiol.2402050606
26. Ghatas MP, Khan MR, Gorgey AS. Skeletal muscle stiffness as measured by magnetic resonance elastography after chronic spinal cord injury: a cross-sectional pilot study. *Neural Regen Res.* Dec 2021;16(12):2486-2493. DOI: http://dx.doi.org/10.4103/1673-5374.313060
27. Xu L, Lin Y, Han JC, Xi ZN, Shen H, Gao PY. Magnetic resonance elastography of brain tumors: preliminary results. *Acta Radiol.* Apr 2007;48(3):327-330. DOI: http://dx.doi.org/10.1080/02841850701199967
28. Murphy MC, Huston J, 3rd, Ehman RL. MR elastography of the brain and its application in neurological diseases. *Neuroimage.* Feb 15 2019;187:176-183. DOI: http://dx.doi.org/10.1016/j.neuroimage.2017.10.008
29. Hughes JD, Fattahi N, Van Gompel J, et al. Higher-Resolution Magnetic Resonance Elastography in Meningiomas to Determine Intratumoral Consistency. *Neurosurgery.* Oct 2015;77(4):653-658; discussion 658-659. DOI: http://dx.doi.org/10.1227/NEU.0000000000000892
30. Sakai N, Takehara Y, Yamashita S, et al. Shear Stiffness of 4 Common Intracranial Tumors Measured Using MR Elastography: Comparison with Intraoperative Consistency Grading. *AJNR. American Journal of Neuroradiology.* 2016;37(10):1851-1859. DOI: http://dx.doi.org/10.3174/ajnr.A4832
31. Aunan-Diop JS, Andersen MCS, Friismose AI, et al. Virtual magnetic resonance elastography predicts the intraoperative consistency of meningiomas. *J Neuroradiol.* 2023;50(4):396-401. DOI: http://dx.doi.org/10.1016/j.neurad.2022.10.006
32. Manduca A, Bayly PJ, Ehman RL, et al. MR elastography: Principles, guidelines, and terminology. *Magn Reson Med.* May 2021;85(5):2377-2390. DOI: http://dx.doi.org/10.1002/mrm.28627
33. Louis DN, Perry A, Wesseling P, et al. The 2021 WHO Classification of Tumors of the Central Nervous System: a summary. *Neuro-oncology.* 2021;23(8):1231-1251. DOI: http://dx.doi.org/10.1093/neuonc/noab106
34. Yushkevich PA, Piven J, Hazlett HC, et al. User-guided 3D active contour segmentation of anatomical structures: significantly improved efficiency and reliability. *Neuroimage.* Jul 1 2006;31(3):1116-1128. DOI: http://dx.doi.org/10.1016/j.neuroimage.2006.01.015
35. Watanabe K, Kakeda S, Yamamoto J, et al. Prediction of hard meningiomas: quantitative evaluation based on the magnetic resonance signal intensity. *Acta Radiol.* Mar 2016;57(3):333-340. DOI: http://dx.doi.org/10.1177/0284185115578323
36. Georgiades CS, Itoh R, Golay X, van Zijl PC, Melhem ER. MR imaging of the human brain at 1.5 T: regional variations in transverse relaxation rates in the cerebral cortex. *AJNR. American Journal of Neuroradiology.* 2001;22(9):1732-1737.
37. Ortega-Porcayo LA, Ballesteros-Zebadúa P, Marrufo-Meléndez OR, et al. Prediction of Mechanical Properties and Subjective Consistency of Meningiomas Using T1-T2 Assessment Versus Fractional Anisotropy. *World Neurosurg.* Dec 2015;84(6):1691-1698. DOI: http://dx.doi.org/10.1016/j.wneu.2015.07.018
38. Qiu S, Jiang W, Alam MS, et al. Viscoelastic characterization of injured brain tissue after controlled cortical impact (CCI) using a mouse model. *J Neurosci Methods.* Jan 15 2020;330:108463. DOI: http://dx.doi.org/10.1016/j.jneumeth.2019.108463
39. Chen L, Chen J, Qiu S, et al. Biodegradable Nanoagents with Short Biological Half-Life for SPECT/PAI/MRI Multimodality Imaging and PTT Therapy of Tumors. *Small.* Jan 2018;14(4). DOI: http://dx.doi.org/10.1002/smll.201702700
40. Gandhe AJ, Hill DL, Studholme C, et al. Combined and three-dimensional rendered multimodal data for planning cranial base surgery: a prospective evaluation. *Neurosurgery.* Sep 1994;35(3):463-470; discussion 471. DOI: http://dx.doi.org/10.1227/00006123-199409000-00015
41. Liu X, Wang Y, Han T, Liu H, Zhou J. Preoperative surgical risk assessment of meningiomas: a narrative review based on MRI radiomics. *Neurosurgical Review.* 2022;46(1):29. DOI: http://dx.doi.org/10.1007/s10143-022-01937-7
42. Zhai Y, Song D, Yang F, et al. Preoperative Prediction of Meningioma Consistency via Machine Learning-Based Radiomics. *Front Oncol.* 2021;11:657288. DOI: http://dx.doi.org/10.3389/fonc.2021.657288
43. Zada G, Yashar P, Robison A, et al. A proposed grading system for standardizing tumor consistency of intracranial meningiomas. *Neurosurg Focus.* Dec 2013;35(6):E1. DOI: http://dx.doi.org/10.3171/2013.8.FOCUS13274
44. Takamura T, Motosugi U, Ogiwara M, et al. Relationship between Shear Stiffness Measured by MR Elastography and Perfusion Metrics Measured by Perfusion CT of Meningiomas. *AJNR. American Journal of Neuroradiology.* 2021;42(7):1216-1222. DOI: http://dx.doi.org/10.3174/ajnr.A7117
45. Della Pepa GM, Menna G, Stifano V, et al. Predicting meningioma consistency and brain-meningioma interface with intraoperative strain ultrasound elastography: a novel application to guide surgical strategy. *Neurosurgical Focus.* 2021;50(1):E15. DOI: http://dx.doi.org/10.3171/2020.10.FOCUS20797
46. Abramczyk H, Imiela A. The biochemical, nanomechanical and chemometric signatures of brain cancer. *Spectrochim Acta A Mol Biomol Spectrosc.* 2018;188. DOI: http://dx.doi.org/10.1016/j.saa.2017.06.037
47. Cieśluk M, Pogoda K, Deptuła P, et al. Nanomechanics and Histopathology as Diagnostic Tools to Characterize Freshly Removed Human Brain Tumors. *Int J Nanomedicine.* 2020;15:7509-7521. DOI: http://dx.doi.org/10.2147/IJN.S270147

SUPPLEMENTAL FILES

Exclusion criteria

(1) inability to finish the whole MR imaging scanning; (2) small tumors require surgery but insufficient for MRE analysis (<15 mm); (3) suboptimal wave image quality (including motion artifacts or low illumination of wave images); (4) diagnosed with a non-meningioma disease according to postoperative pathologic diagnoses; (5) pregnancy

Imaging acquisition protocol

The processing detail was as follows: first, skulls were excluded from T1WI and T2WI using BET2 from the FSL. Then, FA maps, $|G^*|$ maps, and T2WI were realigned to T1WI using SPM12 (Wellcome Trust Centre for Neuroimaging, London, UK), respectively. Both maps were resampled into 2 mm × 2 mm × 2 mm isotropic voxels and normalized to the anatomical standard space defined by the Montreal Neurological Institute (MNI) using Advanced Normalization Tools (ANTs). The whole MRI scan consists of three parts: a structural sequence, an elastography sequence and a functional sequence. Structural sequence consists of a 3D T1WI sequence; the elastography sequence consists of four external vibration frequencies (30 Hz, 40Hz, 50Hz, 60 Hz), each with three orthogonal directions of displacement data; the functional sequence consists of a DTI sequence.

For MRE acquisition, shear waves were introduced intracranially, using a custom-made electromagnetic actuator placed beneath each subject's neck. The power amplitude of mechanical waves was set to 60%. Imaging parameters were as follows: repetition time (TR)/echo time (TE), 4000/65 ms; field of view, 24 cm; acquisition matrix, 80 × 80; slice thickness, 3 mm; contiguous axial slices, 40; motion-encoding gradient, 40 mT/m; 6 motion encoding directions: ±x, ±y, ±z; and phase offsets, 8 (evenly spaced over one period of each vibration frequency). Approximately 18 min of imaging time was needed for MRE portions of exams. For other images, T1W and T2W images were acquired to cover the whole brain using a 3D GRE sequence. For T1W, the imaging parameters were: TR/TE, 1007.37/3.2 ms; slice thickness, 1 mm; slices, 208; field of view, 24 cm × 25.6 cm. For T2W, the parameters were: TR/TE, 5252/111.6 ms; slice thickness, 6.5 mm; slices, 23; field of view, 57.6 cm × 50.1 cm. The diffusion tensor imaging (DTI) data was acquired using a single-shot EPI sequence with the following parameters: TR/TE, 5300/82 ms; noncolinear directions: 32; B0 volume: 1, slice thickness, 1.5 mm.

MRI data construction

For MRE images, All MRE phase images were denoised, unwrapped, and inverted to complex shear modulus, $G^* = G' + iG''$, by an optimization-based phase unwrapping and traveling wave expansion-based neural network (TWENN), where G' was the storage modulus and G'' was the loss modulus. The shear modulus magnitude $|G^*|$ was calculated for final analyses. All modulus maps were filtered by a median filter with a sliding window of 3 × 3 × 3 pixels. For DTI images, the FA and tensor calculation was performed using the tools from the FMRIB Software Library (FSL v6.0, Oxford Centre for Functional MRI of the Brain, Oxford, UK).

Indentation process and data algorithm

Briefly, an 8% strain of the local thickness was indented for a relaxation time of 180 s. Then force-time and displacement-time curves were collected after each ramp-hold test. Maximum four points would be tested for each sample depending on its size, and each measurement took around four minutes.

All force-displacement curves were fitted with the 2-term Prony series, which had three parameters, C_0, C_i, and τ_i, for the ramp ($0 \le t \le t_R$) and relaxation ($t_R \le t$) sections:

$$F = \begin{cases} 8RXV\left(C_0 t - \sum_{i=1}^{2} \tau_i C_i \left(e^{-\frac{t}{\tau_i}} - 1\right)\right) (0 \le t \le t_R) \\ 8RXV\left(C_0 t_R + \sum_{i=1}^{2} \tau_i C_i e^{-\frac{t}{\tau_i}} \left(e^{\frac{t_R}{\tau_i}} - 1\right)\right) (t_R \le t) \end{cases}$$

where F is the related force, R is the radius of the indenter, X is the compensation factor for the infinite half space assumption, V is the indentation velocity. A custom-written MATLAB (MathWorks, Natick, MA, USA) code was included for parameter fitting and optimization. The objective function was set as:

$$f_{obj}(C_0, C_i, \tau_i) = \left[w_1 \sqrt{\frac{1}{n} \sum_{j=1}^{n} \left(F^j - F_{exp}^j\right)^2} \right]_{0 \le t \le t_R} + \left[w_2 \sqrt{\frac{1}{m} \sum_{k=1}^{m} \left(F^k - F_{exp}^k\right)^2} \right]_{t_R \le t} (i = 1,2).$$

where the weights were equal as w_1=w_2=0.5 for the ramp and relaxation in this study. The data points number for each section were n and m, respectively. Then the corresponding instantaneous shear modulus G_0, and long-time shear modulus G_∞ can be computed by the following equation:

$$G_0 = G(0) = C_0 + \sum_{i=1}^{2} C_i, G_\infty = G(\infty) = C_0$$

Supplementary tables

Online Supplemental Data: Statistics of SI ratio (tumor to cerebral cortex SI) on T1WI and T2WI and ROI voxel values for FA, and |G*| images.

Tumor	T1WI		T2WI		FA		|G*|	
consistency	Avg	Std	Avg	Std	Avg	Std	Avg	Std
Soft	1.30	0.20	1.49	0.28	0.30	0.10	1.68	0.35
Firm	1.36	0.35	1.37	0.24	0.35	0.08	2.14	0.47
P	ns (0.34)		ns (0.10)		ns (0.06)		**** (<0.001)	

Supplementary table 1: Patient demographics, presenting symptoms, and tumor characteristics.

Parameter	**Mean / Number**
Age	
Mean (range)	54 (32-76)
Sex	
Female	69 (73%)
Male	25 (27%)
Symptoms	
Headache and dizziness	36 (38.3%)
Epilepsy	10 (10.6%)
Facial numbness	11 (11.7%)
Health check	29 (30.9%)
Others	8 (8.5%)
location	
Convexity	31 (33.0%)
Parafalcine	10 (10.6%)
Tentorial	5 (5.3%)
Sellar region	7 (7.5%)
intraventricular	5 (5.3%)
Anterior fossa	8 (8.5%)
Sphenoid ridge	8 (8.5%)
Foramen magnum	4 (4.3%)
Petroclival	16 (17.0%)
WHO tumor grade	
Grade 1	84 (89.3%)
Fibroblastic	32 (34.0%)
Transitional	10 (10.6%)
Meningothelial	36 (38.3%)
Angiomatous	5 (5.3%)
Secretory	1 (1.1%)
Grade 2	10 (10.7%)
chordoid	1 (1.1%)
Atypical	9 (9.6%)
Size (mm)	37.3 (15.57-74.19)
Intraoperation description	
Soft	7 (7.5%)
Mostly soft	18 (19.1%)
Intermedia	26 (27.7%)
Tenacious	22 (23.4%)
Hard	21 (22.3%)
Operation (Simpson Grade)	
0	4 (4.3%)
I	50 (53.2%)
II	35 (37.2%)
IV	5 (5.3%)

Supplementary table 2: Details of biopsy specimens.

Specimen number	Intraoperative description	T1WI (SI rati0)	T2WI (SI ratio)	DTI (FA)	MRE (|G*|)	Indentation (G0)
1	Mostly soft	0.99	1.50	0.17	1.53	0.82
2	Intermedia	1.19	1.22	0.18	2.16	1.09
3	Intermedia	1.21	1.15	0.22	2.33	1.34
4	Tenacious	1.39	1.47	0.34	1.77	1.01
5	Tenacious	1.51	1.57	0.33	2.15	1.16
6	Tenacious	1.62	1.45	0.3	1.83	1.06
7	Tenacious	1.59	1.48	0.27	2.02	0.9
8	Mostly soft	1.41	1.70	0.46	2.26	0.74
9	Mostly soft	1.41	1.67	0.49	2.22	0.84
10	Firm	1.54	1.50	0.29	2.11	1.48
11	Intermedia	0.93	1.50	0.53	1.04	0.5
12	Intermedia	1.05	1.44	0.34	1.15	0.42
13	Tenacious	1.07	1.24	0.25	1.98	1.29
14	Tenacious	1.12	1.24	0.23	2.27	1.27
15	Soft	0.87	1.38	0.15	1.27	0.49
16	Soft	0.77	1.48	0.11	1.3	0.43
17	Mostly soft	1.11	1.54	0.16	1.7	0.94
18	Tenacious	1.00	1.53	0.22	1.99	1.13
19	Tenacious	1.03	1.33	0.2	2.37	0.83
20	Intermedia	1.56	1.08	0.42	2	0.98
21	Intermedia	1.62	1.03	0.42	2.72	0.99
22	Intermedia	1.48	1.00	0.53	2.54	0.77
23	Tenacious	0.96	1.18	0.27	2.52	1.13
24	Tenacious	0.89	1.11	0.34	2.11	0.92
25	Tenacious	1.09	1.42	0.23	1.93	0.78
26	Tenacious	1.13	1.25	0.24	1.76	0.85
27	Tenacious	1.01	1.27	0.21	2.41	0.97

SI: Signal Intensity

FA: Fractional Anisotropy

|G*|: Shear Modulus Magnitude

G0: instantaneous shear modulus

Supplementary figures

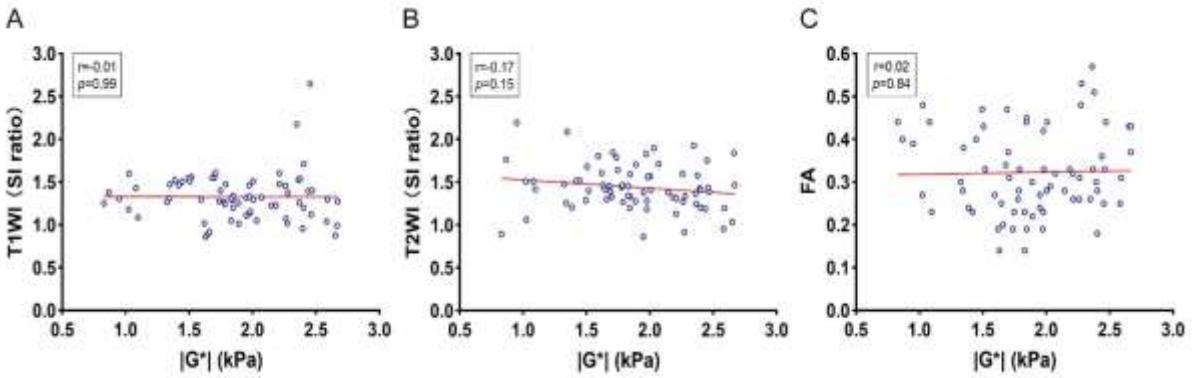

Supplementary FIG 1. Correlation analysis between |G*| values and magnitude of (A) T1WI, (B) T2WI, and (C) FA values.

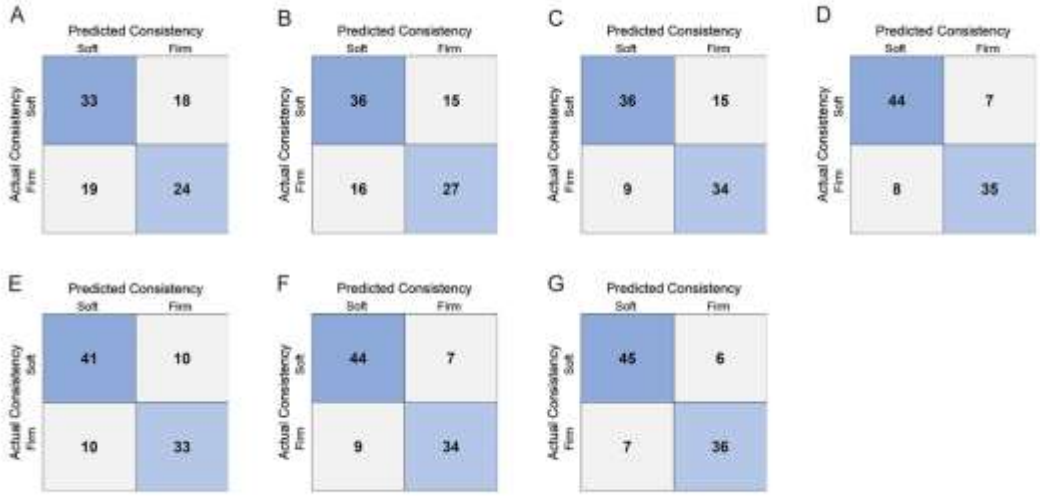

Supplementary FIG 2. Confusion Metrices for Actual tumor consistency and Predicted consistency by (A) T1WI, (B)T2WI, (C)DTI, (D)MRE, (E) MRE-T1WI, (F)MRE-T2WI, (G) MRE-DTI.

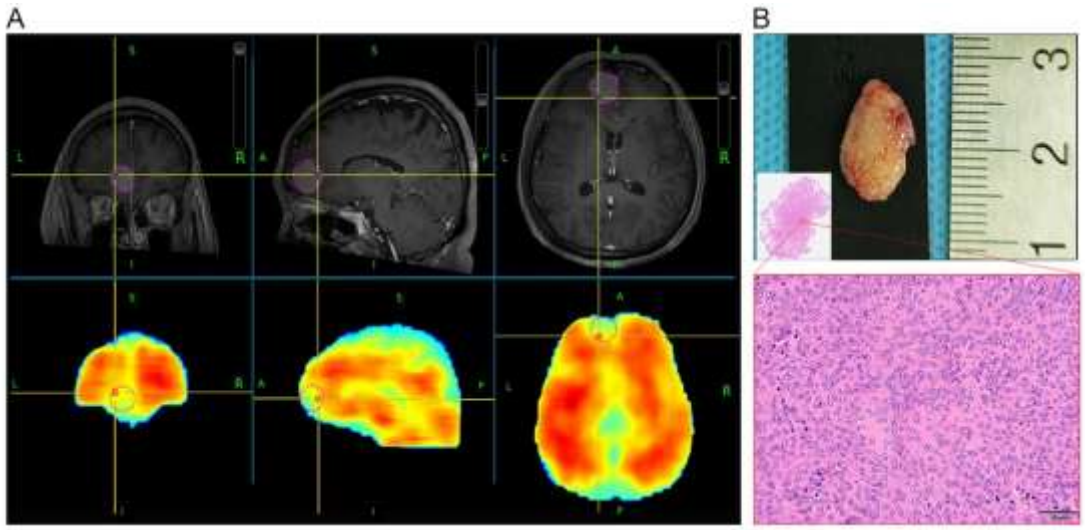

Supplementary FIG 3. Verification of combination modality with intraoperative assessment and indentation measurement. (A) representative image of intraoperative sampling and localization, from left to right, coronal, sagittal and horizontal positions; first row: enhanced T1 sequence, second row: MRE-|G*| map, the purple dashed line is drawn as the tumor area, and the intersection of the yellow solid line is the intraoperative sampling point; (B) Representative images of specimen (top) and its H&E staining (bottom). Scale bar: 50μm.

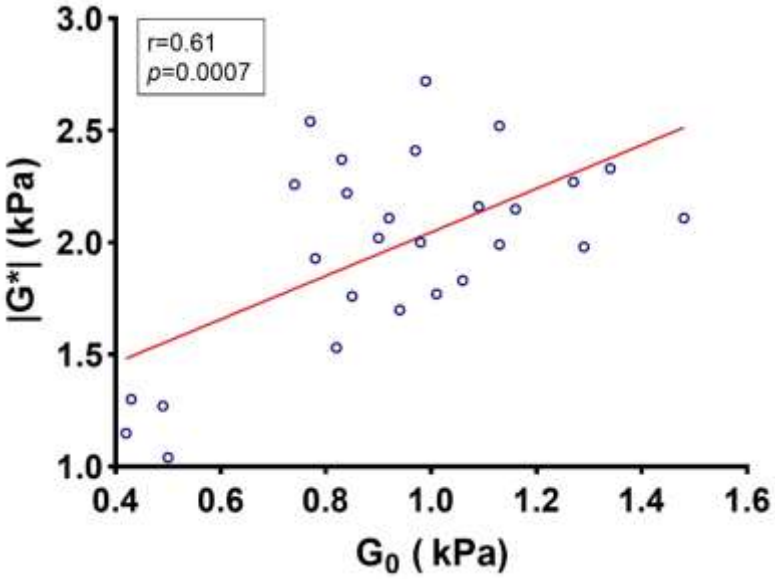

Supplementary FIG 4. Correlation analysis between |G*| and indentation measurement (G0) (r = 0.61, *P* = 0.0007).

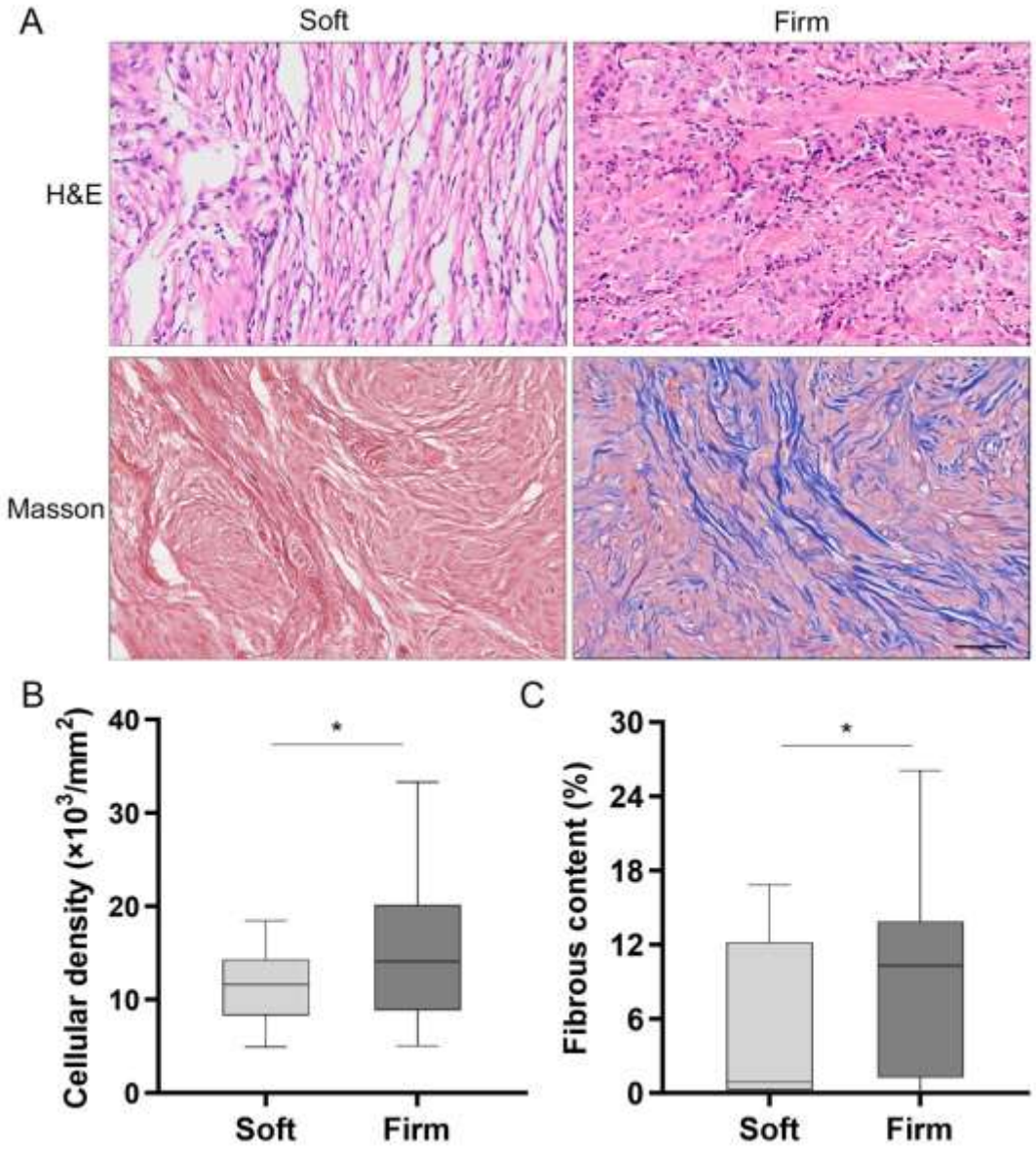

Supplementary FIG 5. Histopathological analysis of tumor sample biopsies. (A) representative images of H&E staining of fibroblastic meningioma (upper row) and Masson staining of transitional meningioma (lower row) between "Soft" and "Firm" groups. Scale bars: 50 μm; (B) Cellular density and (C) Fibrous content in the "Soft" and "Firm" groups.

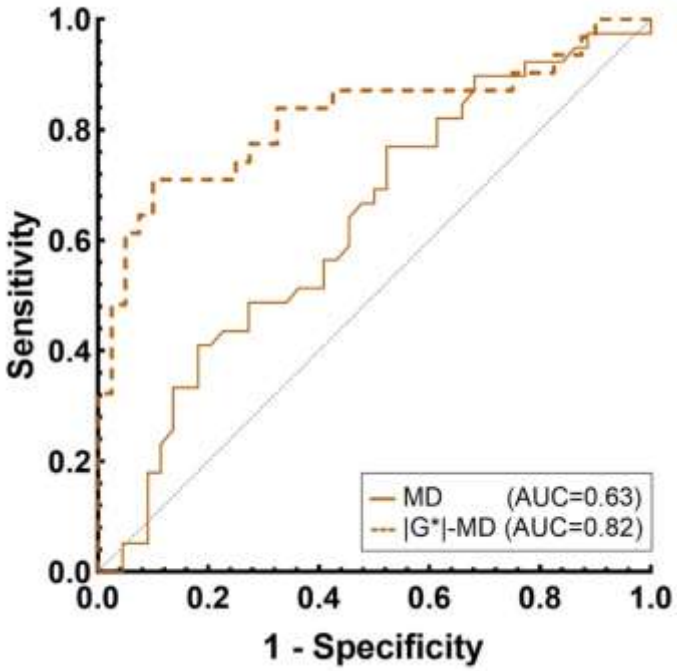

Supplementary FIG 6. ROC curves based on MD and |G*|-MD.

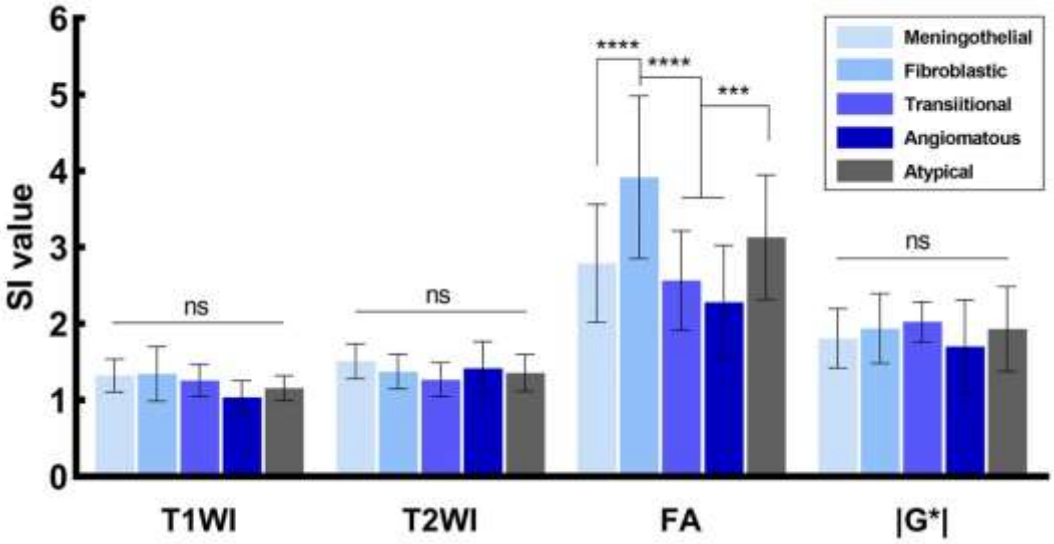

Supplementary FIG 7. Relative SI of each MR sequence image in meningothelial, fibroblastic, transitional, angiomatous, and atypical meningiomas.